The Intramolecular Electric Field Gradient at the ^{14}N-Nucleus in Monofluoroacetonitrile and an Improved Partial r_0-Structure of the Molecule

M. Andolfatto, H. Krause, and D. H. Sutter
Abteilung Chemische Physik im Institut für Physikalische Chemie, Christian-Albrechts-Universität, Kiel, West Germany

M. H. Palmer
Department of Chemistry, West Mains Road, Edinburgh, EH93JJ Scotland

Z. Naturforsch. **43a**, 651–656 (1988); received May 4, 1988

The ^{14}N quadrupole coupling tensor in CH_2FCN and CD_2FCN was determined from the hyperfine splittings of low J rotational transitions to give indirect structural information on the geometry of the CCN chain.

The CCN chain turns out to be slightly bent (2° away from F), in excellent agreement with the result of an earlier ab initio calculation.

Introduction

The microwave rotational spectrum of fluoroacetonitrile and several of its isotopomers has been studied earlier [1–5] to get information on the geometry of the nuclear frame. However, in all evaluations of the microwave data, the CCN-chain was assumed to be linear. In fact, since the central carbon atom of the CCN-chain is close to the a-axis of the molecular moment of inertia tensor (see Fig. 1), its position can be determined only with reduced accuracy from the rotational constants [6].

We therefore took an alternative approach to get information on a possible deviation from linearity in the CCN-chain. First a quantum chemical calculation using a double zeta basis with polarisation functions was carried out at Edinburgh to calculate an ab initio equilibrium structure and the intramolecular electric field gradient at the ^{14}N nucleus. This calculation gave a slightly bent CCN-chain with a CCN-angle of 178° rather than 180° (N-atom bent away from the F-atom). Furthermore, the z-principal axis of the electric field gradient tensor at the nitrogen atom was calculated to fall within 0.2° into the direction of the CN internuclear axis with the z-axis slightly further bent away from the F-atom than the CN-bond.

Reprint requests to Prof. Dr. D. H. Sutter, Institut für Physikalische Chemie, Universität Kiel, Olshausenstraße 40, D-2300 Kiel 1.

The latter result prompted us to approach the problem again from the experimental side by a careful study of the nuclear quadrupole hyperfine structure also of the perdeuterated species.

The basis idea behind this approach is the following: From the result of the quantum chemical calculation assume that the ^{14}N quadrupole coupling tensor is indeed aligned to the CN-bond axis. Determine the orientation of the quadrupole coupling tensor within the molecule from its measured values χ_{aa} and χ_{bb} for the CH_2FCN and the CD_2FCN species and adjust the CCN-angle, keeping all other structural parameters fixed to their r_0-structure values, until the CN internuclear axis and the corresponding principal axis of the quadrupole coupling tensor itself point into the same direction. The resulting CCN-angle should be the correct one.

Experimental

The parent species, CH_2FCN, was prepared by dehydrating monofluoroacetamide powder at low pressure with phosphorous pentoxide [7]:

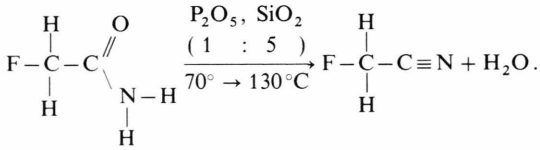

0932-0784 / 88 / 0700-0651 $ 01.30/0. – Please order a reprint rather than making your own copy.

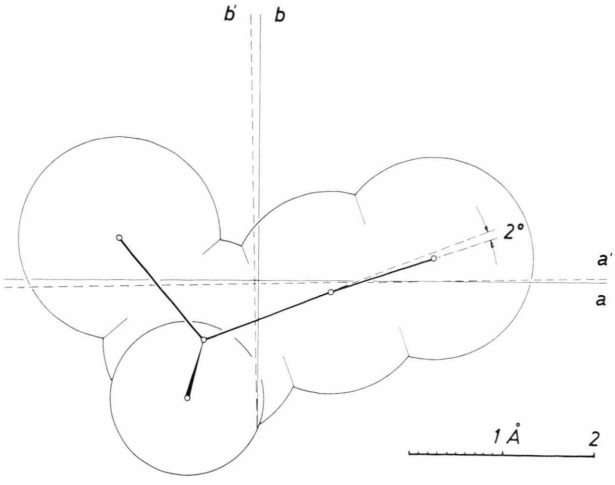

Fig. 1. Upon deuteration the molecular principal inertia axes system is shifted and slightly tilted with respect to the nuclear frame. This tilt leads to changes in the projections of the ^{14}N nuclear quadrupole coupling tensor on the principal inertia axes.

If measured accurately from the hyperfine splittings such as shown in Fig. 2, these changes make it possible to determine the orientation of the nuclear coupling tensor within the molecule. With the additional assumption (prompted by the results of the ab initio calculation) that the ^{14}N quadrupole coupling tensor is closely aligned to the CN bond axis, a 2° bent of the CCN chain can be deduced. The principal inertia axes are denoted by *a*, *b* (nondeuterated species) and by *a'*, *b'* (deuterated species), respectively.

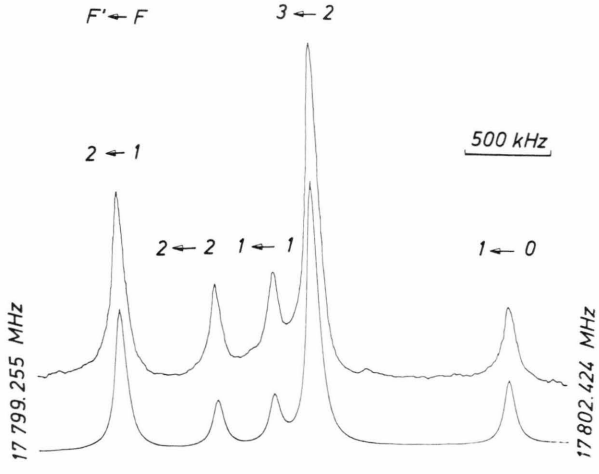

Fig. 2. ^{14}N quadrupole hyperfine splitting of the $1_{11}-2_{12}$ rotational transition of CH_2FCN recorded with the superheterodyne bridge spectrometer with additional 8 kHz Stark-effect modulation. Experimental conditions were: pressure 2 mTorr, temperature −51 °C.

The resulting monofluoroacetonitrile, a colourless liquid at room temperature, was trapped at liq. N_2 temperature and was further purified by vacuum distillation.

The perdeuterated species, CD_2FCN, was prepared in a two-step procedure. In the first step chloroacetonitrile was treated at room temperature with a surplus of heavy water containing a little sodium carbonate to give the di-deuterated species in an exchange reaction [3]:

$$\mathrm{Cl-\overset{H}{\overset{|}{C}}-C\equiv N + D_2O \xrightarrow[20\,^\circ C]{Na_2CO_3} Cl-\overset{D}{\overset{|}{C}}-C\equiv N + H_2O.}$$

The nitrile was separated and the chlorine was exchanged for fluorine following the method given in [8]:

$$\mathrm{Cl-\overset{D}{\overset{|}{C}}-C\equiv N + KF \xrightarrow[170\,^\circ C]{(CH_3)_2NCHO} F-\overset{D}{\overset{|}{C}}-C\equiv N + KCl.}$$

The reaction was carried out by refluxing the chloronitrile and KF in N,N-dimethylformamide as the appropriate aprotic solvent. Again the sample was purified by vacuum distillation.

Two spectrometers were used for the microwave measurements. The hyperfine patterns of the nondeuterated species were recorded with a superheterodyne bridge spectrometer with additional 8 kHz square wave Stark-effect modulation described earlier [9]. In this spectrometer, *J*-band waveguide absorption cells were used with an inner cross section of 1.6 by 3.5 cm in order to reduce wall collision broadening. Full linewidths at half height of typically 70 to 80 kHz were obtained at sample pressures close to 2 mTorr and at sample temperatures close to −50 °C. All hfs-satellites used to fit the ^{14}N quadrupole coupling constants were well resolved. In Fig. 2 we present the recording of the $1_{11} \rightarrow 2_{12}$ rotational transition as an example. A listing of the measured frequencies is presented in Table 1.

The spectra of the deuterated species were recorded using a conventional microwave spectrometer with 33 kHz square wave Stark-effekt modulation and oversized absorption cells with an inner cross section of 1.0 by 5.0 cm. The frequency scans were digitally driven by a minicomputer (Commodore C64), which was also used to perform the averaging up to 200 scans typically [10]. The sample proved to be sufficiently stable to allow steady state measurements.

Table 1. ^{14}N quadrupole hyperfine splittings of some low-J rotational transitions of CH_2FCN. All frequencies are given in units of MHz. The calculated splittings follow from the optimised quadrupole coupling constants presented in Table 3 ($\Delta\nu = \nu - \nu_0$).

$J'\ K'_a\ K'_c - J\ K_a\ K_c$ centre frequency ν_0 [MHz]	$F'-F$	relative intensity	$\Delta\nu_{exp}$ [MHz]	$\Delta\nu_{calc}$ [MHz]
$1_{0\,1} - 0_{0\,0}$	1 – 1	33.3	−0.927	−0.926
9 120.854	2 – 1	55.5	0.186	0.185
	0 – 1	11.1	1.850	1.852
$2_{1\,1} - 1_{1\,0}$	2 – 1	25.0	−0.923	−0.926
18 683.736	2 – 2	8.33	−0.387	−0.382
	1 – 1	8.33	0.023	0.020
	3 – 2	46.6	0.230	0.226
	1 – 0	11.1	1.383	1.379
$2_{1\,2} - 1_{1\,1}$	2 – 1	25.0	−0.919	−0.926
17 800.684	2 – 2	8.33	−0.356	−0.359
	1 – 1	8.33	−0.013	−0.020
	3 – 2	46.6	0.226	0.224
	1 – 0	11.1	1.402	1.399

Table 2. ^{14}N quadrupole hyperfine splittings of some low-J rotational transitions of CD_2FCN. All frequencies are given in MHz. Deuterium quadrupole coupling was neglected in the calculation of the splittings from the coupling constants presented in Table 3 ($\Delta\nu = \nu - \nu_0$).

$J'\ K'_a\ K'_c - J\ K_a\ K_c$ centre frequency ν_0 [MHz]	$F'-F$	relative intensity	$\Delta\nu_{exp}$ [MHz]	$\Delta\nu_{calc}$ [MHz]
$1_{1\,1} - 0_{0\,0}$	0 – 1	11.1	−0.984	−0.987
31 718.598	2 – 1	55.5	−0.098	−0.099
	1 – 1	33.3	0.492	0.492
$2_{1\,1} - 1_{1\,0}$	2 – 1	25.0	−0.944	−0.947
18 179.872	2 – 2	8.33	−0.405	−0.403
	1 – 1	8.33	0.035	0.040
	3 – 2	46.6	0.238	0.232
	1 – 0	11.1	1.406	1.400
$2_{1\,2} - 1_{1\,1}$	2 – 1	25.0	−0.938	−0.947
17 800.684	2 – 2	8.33	−0.354	−0.355
	1 – 1	8.33	−0.052	−0.040
	3 – 2	46.6	0.234	0.228
	1 – 0	11.1	1.436	1.440
$1_{1\,0} - 1_{0\,1}$	1 – 0	11.1	−1.431	−1.440
23 329.274	2 – 2	41.7	−0.283	−0.280
	0 – 1	11.1	0.032	0.040
	1 – 2	13.9	0.261	0.264
	2 – 1	13.9	0.862	0.859
	1 – 1	8.33	1.397	1.400

Typical line widths were close to 150 kHz full width at half height. Thus partial overlap of ^{14}N-hfs-satellites was more frequent and a numerical method already known in ESR-spectroscopy [11] was used for the fast determination of the satellite frequencies. In this

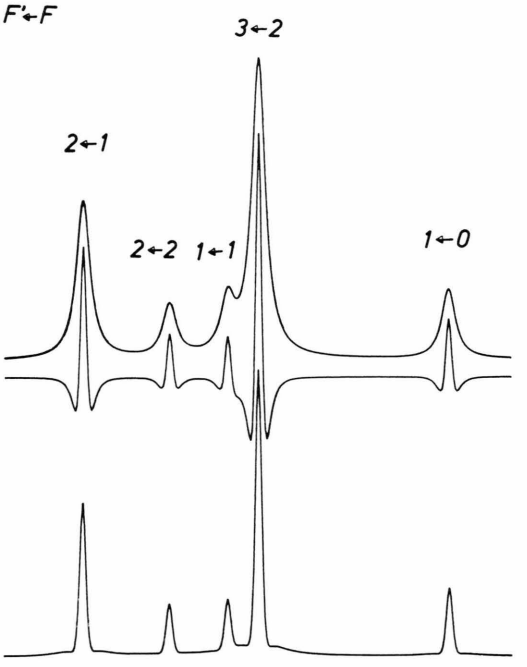

Fig. 3. Simulation of the $1_{10}-2_{11}$ hfs-pattern of CD_2FCN assuming Lorentzian line profiles with 150 kHz full width at half height (upper trace), $-f(\Delta n)^2(y(n+1) - 2\cdot y(n) + y(n-1))$ with $f = 0.7$ and (Δn) the half halfwidth in units of frequency steps (here 10 kHz/step) (centre trace), and the sum of the two traces (lower trace).

method residual noise in the averaged spectrum is further smoothed by a gaussian weighted five point averaging. Then an appropriate multiple of the second derivative of the smoothed line profile is subtracted from the latter, i.e. rather than looking at the curve $y(n)$, where $y(n)$ is used for the amplitude of the observed absorption signal at the n-th point of the digitally swept frequency scan, one looks at the difference

$$\bar{y}(n) - f(\Delta n)^2(\bar{y}(n+1) - 2\,\bar{y}(n) + \bar{y}(n-1)),$$

where $\bar{y}(n)$ are the averaged and smoothed absorption amplitudes and where (Δn) is the observed half width at half height, measured in units of the frequency step of the digital frequency sweep. The factor f is typically chosen close to 0.7.

The procedure is illustrated in Fig. 3, showing a simulated pattern of Lorentzians. Figure 4 gives an experimental example (central section of the $2_{11} \leftarrow 1_{10}$ hfs pattern of CD_2FCN).

In Table 2 we present our measured ^{14}N-hfs-satellite frequency patterns of CD_2FCN.

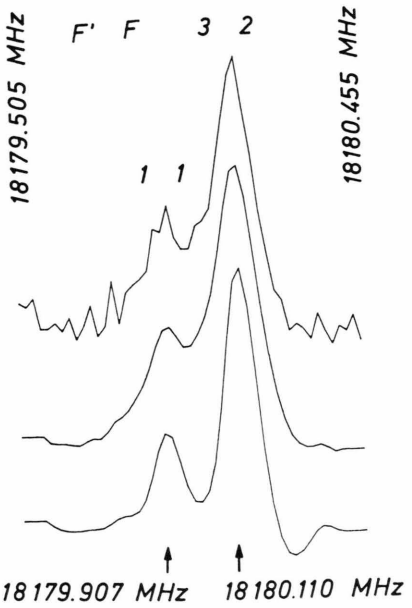

Fig. 4. In praxis additional 5 point gaussian smoothing of the original spectrum is used (second trace) prior to second derivative substraction (lower trace). A computer simulation showed that the peak of the $F \rightarrow F' = 1 \rightarrow 1$ satellite in the lower trace is shifted by about 0.7 kHz towards the more intense $2 \rightarrow 3$ satellite while the latter is essentially unshifted.

Analysis of the hfs-Patterns

The experimental ^{14}N-quadrupole hfs-splittings were analysed as described in a previous publication [12]. Even though there is one sizable off-diagonal element of the quadrupole coupling tensor, χ_{ab}, (all other off-diagonal elements are zero by symmetry), it can not be obtained from the hfs-patterns since its influence on the satellite frequencies is way below the experimental accuracy of our frequency determination. In a simulation its inclusion did lead to shifts in the calculated satellite frequencies, which were all below 0.2 kHz as compared to the noise limited experimental uncertainty of about $\pm$ 5 kHz.

We must note that for CD_2FCN the observed hfs satellites actually consist of narrowly spaced multiplets caused by the additional splitting due to the deuterium quadrupole hyperfine interaction. However, in all transitions reported in Table 2 these subsatellites probably fall within a $\pm$ 50 kHz range around the satellite frequency calculated under the neglect of deuterium quadrupole coupling and they leave the intensity weighted means of the corresponding submultiplet unchanged. This justified the neglect of deuterium quadrupole coupling in the final analysis of the hfs-patterns. The $\pm$ 50 kHz bounds were estimated from a prediction calculated with an assumed deuterium quadrupole coupling tensor with $\chi_{zz} = +0.2$ MHz and $\chi_{xx} = \chi_{yy} = -0.1$ MHz (z-axis parallel to the CD bond). These values for the deuterium coupling were chosen similar to those reported recently for 4-D-pyridine [13].

Deuterium quadrupole coupling as well as larger Stark-modulation broadening partly accounts for the increased linewidths observed for CD_2FCN.

Our optimised quadrupole coupling constants are presented in Table 3. Also given for comparison are the values determined earlier by Kasten and Dreizler in their microwave Fourier-transform study of the nondeuterated species.

Table 3. ^{14}N quadrupole coupling constants from a least squares fit of χ_+ and χ_- (top rows) to the hfs-splittings presented in Tables 1 and 2. The diagonal elements of the ^{14}N quadrupole coupling tensor in its own principal axes system (z-axis assumed to fall into the direction of the CN internuclear axis, y-axis perpendicular to the heavy atom plane) follow within the iterative procedure described in the text, which leads to an angle of 18.56° between the a-axis and the CN-bond axis and to an off-diagonal element of the quadrupole coupling tensor χ_{ab}(H) = − 2.119 MHz. The quadrupole coupling tensor elements are related to the intramolecular field gradient tensor by $\chi_{aa} = eQV_{aa}/h$ etc. with e = proton charge, Q = nuclear quadrupole moment of the ^{14}N nucleus, h = Planck's constant and V_{aa} the second derivative of the intramolecular Coulomb potential in direction of the a-axis taken at the position of the ^{14}N nucleus. For comparison, the quadrupole coupling constants determined earlier by Kasten and Dreizler are given in brackets [3].

	CH_2FCN	CD_2FCN
$\chi_+ = \chi_{bb} + \chi_{cc}$	3.7039 ± 0.0026 MHz (3.707 ± 0.004 MHz)	3.7858 ± 0.0048 MHz
$\chi_- = \chi_{bb} + \chi_{cc}$	0.0796 ± 0.0046 MHz (0.071 ± 0.004 MHz)	0.1603 ± 0.0066 MHz
χ_{aa}	− 3.7039 ± 0.0026 MHz (− 3.707 ± 0.004 MHz)	− 3.7858 ± 0.0049 MHz
χ_{bb}	+ 1.8918 ± 0.0026 MHz (1.889 ± 0.004 MHz)	+ 1.9731 ± 0.0041 MHz
χ_{cc}	+ 1.8122 ± 0.0037 MHz (1.818 ± 0.004 MHz)	+ 1.8127 ± 0.0064 MHz
χ_{zz}	− 4.416 MHz	
χ_{xx}	+ 2.604 MHz	
χ_{yy}	+ 1.812 MHz	

Discussion

As already indicated in the introduction, we decided to use the observed quadrupole coupling constants

as additional information for an improved partial r_0-structure determination (also called "effective structure" [14]). In detail we proceeded by an iterative cycle as follows.

In the first step of the cycle we used the known rotational constants of CH_2FCN [5], CD_2FCN [3], and $CH_2FC^{15}N$ [4] for a routine nonlinear least squares fit of the CF- and the CH-bond distances and of the angles $\measuredangle$ HCC, $\measuredangle$ FCC, and the dihedral angle $\measuredangle$ HCC/FCC. Correlation precluded a fit of more parameters, although nine experimental rotational constants were available. The CC-bond and the CN-bond were fixed to 1.460 and 1.158 Å, respectively [1, 3], and the CCN angle was set to 180° (linear chain) but was open for later variation. V. Typkes program MWSTR was used for this fit [15].

In the second step, the CCN bond angle was varied from 180° to 177° in steps of 0.2°, while all other structural parameters were frozen to their values from step 1. For each CCN angle the orientation of the CN-bond with respect to the *a*-axis of the molecular principal inertia tensor was calculated. Furthermore for each of these structures the tilt of the moment of inertia tensor upon double-deuteration, τ, was calculated. This tilt angle was then used to calculate a value for the off-diagonal element of the ^{14}N quadrupole coupling tensor, $\chi_{ab}(\mathrm{H})$, according

$$\chi_{ab}(\mathrm{H}) = \frac{\chi_{aa}(\mathrm{D}) - \cos^2(\tau)\cdot\chi_{aa}(\mathrm{H}) - \sin^2(\tau)\cdot\chi_{bb}(\mathrm{H})}{\sin(2\cdot\tau)}, \quad (1)$$

or

$$\chi_{ab}(\mathrm{H}) = \frac{\chi_{bb}(\mathrm{D}) - \sin^2(\tau)\cdot\chi_{aa}(\mathrm{H}) - \cos^2(\tau)\cdot\chi_{bb}(\mathrm{H})}{\sin(2\cdot\tau)}, \quad (2)$$

(the indices H and D refer to the isotopic species, CH_2FCN and CD_2FCN, respectively).

Finally, the average $\chi_{ab}(\mathrm{H})$-value from (1) and (2) was used together with the experimental values for $\chi_{aa}(\mathrm{H})$ and $\chi_{bb}(\mathrm{H})$ to calculate the corresponding angle between the *z*-principal axis of the ^{14}N quadrupole coupling tensor and the *a*-axis of the principal inertia tensor $\measuredangle(a, z)$:

$$\tan(2\cdot\measuredangle(a,z)) = \frac{2\cdot\chi_{ab}(\mathrm{H})}{\chi_{aa}(\mathrm{H}) - \chi_{bb}(\mathrm{H})}. \quad (3)$$

By this procedure a set of $\measuredangle(a, \mathrm{CN})$-angles and of $\measuredangle(a, z)$-angles was obtained, each a function of the corresponding CCN-angle. According to our basic assumption, the "correct" CCN-angle should be obtained from the intercept of the $\measuredangle(a, \mathrm{CN})$-function and of the $\measuredangle(a, z)$-function. This value, 178.45° in the first cycle, was then used as input (rather than 180°) for a new "step one" of a second cycle and so forth until selfconsistency was reached for a CCN-bond angle of 178° in close agreement with the ab initio result (N-atom slightly bent away from the F atom).

Table 4. Comparison of our partial r_0-structure and our ab initio equilibrium structure. For the r_0-structure determination, r(CN) and r(CC) were fixed to average values observed for related molecules [2, 4], and the CCN bond angle was optimised for best agreement with the observed ^{14}N quadrupole coupling tensor elements of CH_2FCN and CD_2FCN. As compared to the linear configuration, the CN bond is bent away from the electronegative F-atom by 2°.

Given uncertainties are single standard deviations of the rigid rotor least squares fit to the observed effective rotational constants of CH_2FCN, CD_2FCN, and $CH_2FCN^{14}N$.

	Partial r_0-structure	ab initio equilibrium structure (double-zeta + d)$_{C,N}$
r(CN)/Å	(1.158)	1.1358
r(CC)/Å	(1.460)	1.4813
r(FC)/Å	1.3837 ± 0.0008	1.3619
r(CH)/Å	1.0874 ± 0.0027	1.0881
$\measuredangle$ CCH	110.11° ± 0.66°	109.13°
$\measuredangle$ CCF	110.24° ± 0.03°	110.27°
$\measuredangle$ CCH/CCF	120.53° ± 0.31°	119.66°
$\measuredangle$ CCN	178°	177.97°

Table 5. Correlation of the structural parameters of monofluoroacetonitrile in the least squares fit to the nine observed rotational constants presented in Table 6.

r(CF)	1.000				
$\measuredangle$ FCC	−0.926	1.000			
r(CH)	−0.776	0.828	1.000		
$\measuredangle$ HCC	0.942	−0.842	−0.755	1.000	
$\measuredangle$ HCC/FCC	0.471	−0.645	−0.907	0.430	1.000

In Table 4 we present the partial r_0-structure finally obtained from our procedure together with our ab initio structure. In Table 5 we present the corresponding correlation matrix. We note that the standard deviations of our fit are considerably smaller than those reported in [4].

Finally, in Table 6, we present a comparison of the observed effective rotational constants for the CH_2FCN, CD_2FCN, and $CH_2FC^{15}N$ isotopic species with the corresponding rotational constants calculated within the rigid rotor model from our partial r_0-structure presented in Table 4. With deviations on the order of MHz and below, both sets are in fair agreement. The differences are due to zero point vibrations, and to a minor degree to the fact that r(CN)

Table 6. Observed effective vibronic ground state rotational constants of monofluoroacetonitrile CH_2FCN [5], CD_2FCN ([3] and this work) and $CH_2FC^{15}N$ ([4], Table 4), and the corresponding rigid rotor rotational constants calculated from our structure presented in Table 4.

	CH_2FCN	CD_2FCN	$CH_2FC^{15}N$
A_0, exp/MHz	36 578.6697 (98)	27 524.070 (57)	36 417.743 (104)
A calc/MHz	36 576.849	27 524.113	36 419.525
B_0, exp/MHz	4 781.2847 (9)	4 661.770 (21)	4 626.490 (4)
B calc/MHz	4 779.894	4663.400	4 625.152
C_0 exp/MHz	4 339.7246 (9)	4 194.620 (10)	4 209.687 (4)
C calc/MHz	4 340.666	4 193.978	4 210.581

and r(CC) were held fixed (With the present set of rotational constants these two bond distances are strongly correlated with a longer CC-bond going along with a shorter CN-bond and vice versa).

Since "effective structures" as determined here lead to bond distances which are typically few thousends of an Å longer than the equilibrium values (see [6], p. 678), the agreement between the two structures presented in Table 4 appears already reasonable with the possible exception of the CC-bond distance and the CN-bond distance. Investigation of the carbon-13 species, currently under way in the group of A. Guarnieri at Kiel, will possibly resolve the remaining discrepancy.

The final results were: total energy −230.79611 a.u.; dipole moment 3.43 D; populations, N: 7.1194, C(N): 6.1109, C(F): 5.8665, H: 0.8232; the final structure (Table 4) can be compared with the corresponding ones obtained with the same basis set for CH_3CN (CN: 1.1286; CC: 1.4659; CH: 1.0810 Å; CCH: 109.69°), CF_3CN (CN: 1.138; CC: 1.4716; CF: 1.3616 Å); CCF: 111.04°), and CHF_2CN (CN: 1.1343; CC: 1.4893; CH: 1.0860; CF: 1.3351 Å; NCC: 177.38°; CCH: 110.65°; CCF: 109.63°).

In both the cases of CH_2FCN and CHF_2CN, the N is bent away from the F atom(s), with NCCF 180° and ±120.54° respectively, and HCF 108.97° and 109.22° respectively.

Appendix

The double zeta (9S 5p/4S) basis for C, N/H [16] was augmented at N, C by d-polarisation functions (exponents 0.85, 0.72) to allow additional flexibility in the CCN skeleton; the F basis set was split valence [16].

Acknowledgement

We would like to thank Prof. Dr. A. Guarnieri for critically reading the manuscript. The Kiel group gratefully acknowledges financial support by Deutsche Forschungsgemeinschaft and by the Fonds der Chemischen Industrie.

[1] B. E. Job and J. Sheridan, Nature London **192,** 160 (1961).
[2] J. D. Graybeal and D. W. Roe, J. Chem. Phys. **37,** 2503 (1962).
[3] W. Kasten, H. Dreizler, B. E. Job, and J. Sheridan, Z. Naturforsch. **38a,** 1015 (1983).
[4] H. Zerbe and A. Guarnieri, Z. Naturforsch. **42a,** 1275 (1987).
[5] A. Guarnieri and G. Tolkmit, Z. Naturforsch. **39a,** 853 (1984).
[6] W. Gordy and R. L. Cook, Microwave Molecular Spectra, 3rd Edition, Wiley Interscience, New York 1984, p. 698.
[7] H. Gilman and R. G. Jones, J. Amer. Chem. Soc. **65,** 1458 (1943).
[8] Houben-Weyl, Methoden der Organischen Chemie, Vol. V, p. 150.
[9] W. H. Stolze, M. Stolze, D. Hübner, and D. H. Sutter, Z. Naturforsch. **37a,** 1165 (1982).
[10] W. H. Stolze, PhD Thesis, Universität Kiel (1988).
[11] L. C. Allen, H. M. Gladney, and S. H. Glarum, J. Chem. Phys. **40,** 3135 (1964).
[12] M. Stolze, D. Hübner, and D. H. Sutter, Z. Naturforsch. **36a,** 886 (1981).
[13] N. Heineking, H. Dreizler, and R. Schwarz, Z. Naturforsch. **41a,** 1210 (1986).
[14] For a detailed presentation of the different methods used to derive molecular structures from spectroscopic data we refer to Chap. XIII of the excellent textbook by W. Gordy and R. L. Cook (see [6]).
[15] V. Typkes program is based on the methods presented by P. Noesberger, A. Bauder, and Hs. H. Günthard, Chem. Phys. **1,** 418 (1973).
[16] T. H. Dunning, J. Chem. Phys. **53,** 2823 (1970).